applied sciences

MDPI

Article

Power System State Estimation Approach Considering Transmission Line Temperature

Qingwen Xu [1], Hengxu Zhang [1], Yongji Cao [2,*], Hao Qin [1] and Zhimin Gao [1]

[1] Key Laboratory of Power System Intelligent Dispatch and Control of the Ministry of Education, Shandong University, Jinan 250061, China
[2] Department of Electrical Engineering, Technical University of Denmark, 2800 Kongens Lyngby, Denmark
* Correspondence: caoyong@dtu.dk

Abstract: The transmission line parameters vary with the change of temperature, which has a significant impact on power system state estimation (SE). Based on the theory of electro-thermal coordination (ETC), this paper proposes two ETC-SE approaches with the consideration of transmission line temperature. The heat balance equation (HBE) is combined with the conventional weighted least square SE for establishing an ETC-SE model. Moreover, an augmented Jacobian ETC-SE approach is developed by integrating the HBE into pseudo measurements and the line temperature into state vectors. The Jacobian matrix is augmented correspondingly and the partial differential coefficients of measurements to line temperature are provided, which enables to calculate line temperature and voltage phasors simultaneously. Furthermore, in order to accelerate the solving process, an improved two-step ETC-SE algorithm is proposed, in which the SE and temperature estimation are decoupled and solved via alternate iteration. The effectiveness of the proposed ETC-SE approaches is verified by the IEEE 14-, 39-, and 118-bus systems. The results show that the proposed ETC-SE approach is effective to reduce the calculation errors and possesses good convergence performance with varying environmental circumstances and ill-conditioned branches.

Keywords: state estimation; electro-thermal coordination; heat balance equation; transmission line temperature

Citation: Xu, Q.; Zhang, H.; Cao, Y.; Qin, H.; Gao, Z. Power System State Estimation Approach Considering Transmission Line Temperature. *Appl. Sci.* **2022**, *12*, 10171. https://doi.org/10.3390/app121910171

Academic Editor: Jožef Ritonja

Received: 8 September 2022
Accepted: 7 October 2022
Published: 10 October 2022

1. Introduction

In recent years, the development of renewable generations and power electronic devices has been accelerated [1,2]. The outputs of renewable generations are uncertain and fluctuant [3]. In addition, the response velocity of power electronic devices is faster than conventional synchronous generators [4]. With the development of renewable generations and power electronic devices, states of the power system are becoming more complicated and variable. The estimation of power system states is necessary under both the normal operation and contingencies [5,6]. Therefore, it is necessary to attain power system states for the security and economic operation.

State estimation (SE) serves as an essential part in the advanced application of the energy management system, whose main role is to provide a reliable and sufficient database for other applications, e.g., power flow analysis, economic dispatch, and stability control [7,8]. The main factors influencing the accuracy of SE include measuring devices and transmission line parameters [9]. The rapid development of the phasor measurement unit (PMU) and advanced communication infrastructure has improved the precision of measured data [10]. However, parameters of transmission lines are often regarded as constant values and the effect of line temperature is ignored, which will result in parameter inaccuracy and has become an obstacle restricting the precision of state estimation. Failure to modify line parameters according to temperature may lead to significant errors in the calculation of power flow and network loss, whose errors may even exceed 30% [11,12].

Electro-thermal coordination (ETC) that combines line temperature with electrical quantities is capable of decreasing temperature-dependent errors in power flow, SE, and related analysis [13]. The basic ETC principle is to establish an analytical relationship of the line temperature, current, and weather conditions through the heat balance equation (HBE) [14]. Line temperature is calculated by the HBE, and then line parameters can be corrected correspondingly.

Studies on ETC in the power system mainly focus on the thermal rating [15–17], power flow analysis [18–20], and estimation of power system states and temperature [21–24]. Based on dynamic thermal models, a real-time thermal rating method for the lines of the distribution network was proposed [15]. Considering the scenarios of normal operation and contingency, the performance of different real-time line monitoring devices on dynamic thermal rating has been assessed [16]. The dynamic thermal-line rating is conducted using online measurements so as to adjust the operational tripping scheme [17]. In addition, a temperature-dependent power flow algorithm was proposed, where the augmented equation set is solved by the Newton–Raphson method [18]. ETC was combined with optimal power flow, on which economic losses can be reduced [19]. With the consideration of temperature-related resistance and thermal rating, a weather-based optimal power algorithm was designed [20].

Moreover, the influence of temperature on SE performance was analyzed, and the results verify that the errors caused by temperature are not negligible [21]. Using Monte Carlo simulation and a variance reduction method, the critical line temperature in the presence of fluctuating power flows was estimated probabilistically [22]. Based on the analytical solution and numerical weather prediction, a simulation method for the evolution of line temperature was proposed [23]. In addition, a constrained nonlinear optimization model for estimating both the voltage phasors and the temperature of transmission line conductors was established and solved by a predictor–corrector interior point method [24].

With regard to SE, there are extensive efforts devoted to its performance modification techniques [25–33]. A hybrid state estimator using the measurements of remote terminal units (RTUs) and PMUs was designed with bad data detection [25]. Considering the parameter errors and bad measurements, a robust SE method was proposed, which is formulated as a tractable mixed-integer linear programming optimization problem [26]. The distributed SE operates locally with minimal data exchange with neighbors and is applicable for multi-area power systems [27]. Based on the iterative reweight least square algorithm, a distributed SE method was proposed, where the improved alternating direction method of multipliers is utilized to improve result accuracy and convergence speed [28]. In addition, the placement of PMUs was optimized to improve the reliability of SE results [29]. Considering bad data and missing measurements, a multi-objective PMU allocation method was presented for achieving the desired accuracy of SE [30]. The unscented Kalman filter was used to estimate the states of a permanent magnet synchronous motor (PMSM) [31]. In addition, a multi-area distributed SE method was proposed with the use of the data-driven Kalman filter [32]. In order to estimate the states of electric vehicle batteries (EVBs), a robust adaptive filter, an adaptive smooth variable structure filter has been designed [33]. The aforementioned SE methods are summarized in Table 1.

For the sake of reducing the temperature-dependent errors, this paper proposes two ETC-SE approaches with the consideration of transmission line temperature. In the augmented Jacobian ETC-SE (AJ-ETC-SE) approach, line temperature is integrated into state variables, and the HBE serves as a pseudo-measurement. Compared to the weighted least square SE (WLS-SE), the dimension of the measurement and state vectors increases, but the equation set is still overdetermined. Additionally, the elements in the augmented Jacobian matrix are provided, and the equation set is solved using the Newton method. On the other hand, the improved two-step ETC-SE (ITS-ETC-SE) approach decouples the calculation process of voltage phasors and line parameters. Compared with the AJ-ETC-SE approach, the SE and temperature estimation are solved via alternate iteration so as to reduce the iteration number and computation time.

Table 1. Comparative literature survey on state-of-the-art SE methods.

Reference	Method/Model	Characteristic/Application
[15]	State space model	Thermal rating with demand response
[16]	HBE	Thermal rating to detect line overload
[17]	Transient thermal rating equation	Thermal rating with tripping scheme
[18]	Newton-Raphson method	Temperature-dependent power flow
[19]	ETC	Power flow analysis for system security
[20]	Primal-dual interior point method	Weather-based optimal power flow
[21]	ETC	Influence analysis of temperature on SE
[22]	Monte Carlo method	Probabilistic simulation of line temperature
[23]	Analytical solution method	Simulation of line temperature
[24]	Predictor-corrector interior point algorithm	Line temperature estimation
[25]	Weighted least square SE	SE considering bad data detection
[26]	Robust optimization	SE considering parameter errors
[27]	Bilinear optimization	SE with nonlinear measurements
[28]	Iterative reweight least squares method	SE with bad data
[29]	WLS	SE for the placement of PMUs
[30]	Modified Jaya algorithm	SE for the placement of PMUs
[31]	Unscented Kalman filter	SE for PMSM
[32]	Data-driven Kalman filter	Multi-area and distributed SE
[33]	Adaptive smooth variable structure filter	SE for EVBs

Therefore, the main contributions of this paper are three-fold. Firstly, an ETC-SE model integrating the HBE and WLS-SE is established to consider the impact of line temperature on power system states. Secondly, the AJ-ETC-SE approach is proposed to simultaneously solve the problems of SE and temperature estimation through an augmented Jacobian matrix. Finally, the ITS-ETC-SE approach is proposed to accelerate the solving process, in which the SE and temperature estimation are decoupled and solved via alternate iteration.

The rest of this paper is organized as follows. Section 2 develops an ETC-SE model with the consideration of the HBE and meteorological data. The procedure of the AJ-ETC-SE approach is presented in Section 3. Moreover, Section 4 gives the ITS-ETC-SE approach. The case studies of the IEEE 14-, 39-, and 118-bus systems are conducted in Section 5. Finally, conclusions are drawn in Section 6.

2. ETC-SE Model

2.1. Measurement and State Vector of the ETC-SE Model

The lumped parameter model of the transmission line l is shown in Figure 1, supposing that the two terminal ends are bus i and j, respectively. P_i and Q_i are the active and reactive power injection of bus i, respectively; P_j and Q_j are the active and reactive power injection of bus j, respectively; P_{ij} and Q_{ij} are the active and reactive power flow of the line l, respectively; U_i and U_j are the voltage amplitudes of bus i and j, respectively; $I_{ij,real}$ and $I_{ij,imag}$ are the real and image parts of the current from bus i to bus j, respectively; $I_{ji,real}$ and $I_{ji,imag}$ are the real and image parts of the current from bus j to bus i, respectively; g_{ij} and b_{ij} are the mutual conductance and susceptance of the line l, respectively; and $g_{ij,c}$ and $b_{ij,c}$ are the self-conductance and susceptance of the line l, respectively.

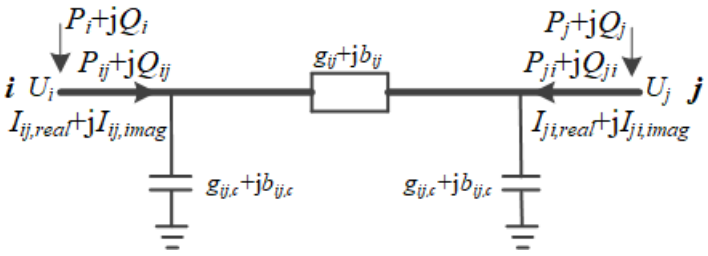

Figure 1. Lumped model of the transmission line.

Considering the influence of line temperature, the vectors of measurements and states are augmented in the ETC-SE model. The augmented measurement vector z_{aug} can be represented as,

$$z_{aug} = [z_{elec}\ z_{meteo}]^T \tag{1}$$

with

$$z_{elec} = [U_i\ \ P_i\ \ Q_i\ \ P_{ij}\ \ Q_{ij}]^T \tag{2}$$

$$z_{meteo} = [Q_{solar}\ \ \vartheta\ \ V_w\ \ T_a\ \ \phi]^T \tag{3}$$

where z_{elec} and z_{meteo} are the measurement vectors of electrical and meteorological quantities, respectively; Q_{solar}, ϑ, V_w, T_a, and ϕ are the solar irradiation intensity, solar incidence angle, wind speed, ambient temperature, and wind directions, respectively.

Then, the augmented measurement function vector h_{aug} can be represented as,

$$h_{aug} = [h_{elec}\ \ h_{HBE}]^T \tag{4}$$

where h_{elec} and h_{HBE} are the measurement function vectors of electrical and HBE, respectively.

In addition, the augmented state vector x_{aug} can be represented as,

$$x_{aug} = [U\ \theta\ T]^T \tag{5}$$

where U, θ, and T are the voltage magnitude, voltage angle, and line temperature vectors, respectively.

2.2. Measurement Functions of the ETC-SE Model

With the consideration of the line temperature, the measurement functions are modified in the proposed ETC-SE model, and can be listed as,

$$\begin{cases} U_i = U_i \\ \theta_i = \theta_i \\ P_i = U_i \sum\limits_{j\in i} U_j[G_{ij}(T)\cos\theta_{ij} + B_{ij}(T)\sin\theta_{ij}] = 0 \\ Q_i = U_i \sum\limits_{j\in i} U_j[G_{ij}(T)\sin\theta_{ij} - B_{ij}(T)\cos\theta_{ij}] = 0 \\ P_{ij} = U_i^2(g + g_c) - U_iU_jg\cos\theta_{ij} - U_iU_jb\sin\theta_{ij} \\ Q_{ij} = -U_i^2(b + b_c) - U_iU_jg\sin\theta_{ij} + U_iU_jb\cos\theta_{ij} \end{cases} \tag{6}$$

with

$$G_{ij}(T) = -g_{ij}(T) = -\frac{R_{ij}(T)}{R_{ij}(T)^2 + {X_{ij}}^2} \tag{7}$$

$$B_{ij}(T) = -b_{ij}(T) = \frac{X_{ij}}{R_{ij}(T)^2 + {X_{ij}}^2} \tag{8}$$

The measurement functions are the nonlinear functions of line temperatures, which can be calculated via the HBE. The meteorological data z_{meteo} are used to calculate the heat parameters, which can be represented as [10],

$$h_{HBE} = I^2R(T) + q_s - q_c(T) - q_r(T) = 0 \tag{9}$$

$$q_c = A_c(T - T_a) \tag{10}$$

$$q_r = A_r[(T + 273)^4 - (T_a + 273)^4] \tag{11}$$

$$R(T) = R_r[1 + \alpha_l(T - T_d)] \tag{12}$$

where R is the unit resistance of transmission line; q_s, q_c, and q_r are the solar heat gain, convective heat loss, and radiated heat loss, respectively; A_c and A_r are the coefficients for

convective heat loss and radiated heat loss, respectively; α is the temperature coefficient of resistance; T_d is the reference temperature; R_r is the rated resistance at temperature T_d.

3. Augmented JACOBIAN ETC-SE Approach

3.1. Augmented Jacobian ETC-SE

The AJ-ETC-SE approach calculates line temperature and voltage phasors simultaneously. The state vector is consistent with $\boldsymbol{x}_{aug}$, and the augmented measurement vector $\boldsymbol{z}_{aug}$ is expressed as,

$$\boldsymbol{z}_{aug} = \begin{bmatrix} u_i & P_i & Q_i & P_{ij} & Q_{ij} & 0 \end{bmatrix}^T \tag{13}$$

The HBE is taken as pseudo measurements into the measurement vector like zero-injection measurements. Additionally, the measurement equations of the AJ-ETC-SE approach can be written as,

$$\boldsymbol{z}_{aug} = \boldsymbol{h}(\boldsymbol{x}_{aug}) + \boldsymbol{v}_z \tag{14}$$

where $\boldsymbol{v}_z$ is the vector of measurement errors.

Using Taylor expansion at the initial value, $\boldsymbol{h}(\boldsymbol{x}_{aug})$ can be expressed as,

$$\boldsymbol{h}(\boldsymbol{x}_{aug}) = \boldsymbol{h}(\boldsymbol{x}_{aug,0}) + \boldsymbol{H}(\boldsymbol{x}_{aug,0})\Delta\boldsymbol{x}_{aug} \tag{15}$$

where $\Delta\boldsymbol{x}_{aug}$ and $\boldsymbol{H}(\boldsymbol{x}_{aug,0})$ are the correction vector and Jacobian matrix, respectively.

In order to minimize the residuals between $\boldsymbol{z}_{aug}$ and $\boldsymbol{h}(\boldsymbol{x}_{aug})$, the objective function is established by WLS and expressed as,

$$J(\boldsymbol{x}_{aug}) = [\boldsymbol{z}_{aug} - \boldsymbol{h}(\boldsymbol{x}_{aug})]^T \boldsymbol{R}^{-1} [\boldsymbol{z}_{aug} - \boldsymbol{h}(\boldsymbol{x}_{aug})] \tag{16}$$

where $\boldsymbol{R}$ is the weighting matrix.

By substituting (15) into (16), the correction vector in the kth step $\Delta\boldsymbol{x}_{aug,k}$ can be written as,

$$\Delta\boldsymbol{x}_{aug,k} = [\boldsymbol{H}^T(\boldsymbol{x}_{aug,k})\boldsymbol{R}^{-1}\boldsymbol{H}(\boldsymbol{x}_{aug,k})]^{-1} \cdot \boldsymbol{H}^T(\boldsymbol{x}_{aug,k})\boldsymbol{R}^{-1}\Delta\boldsymbol{z}_{aug,k} \tag{17}$$

Thus, the state vector in the kth step $\boldsymbol{x}_{aug,k}$ can be calculated as,

$$\boldsymbol{x}_{aug,k+1} = \boldsymbol{x}_{aug,k} + \Delta\boldsymbol{x}_{aug,k} \tag{18}$$

3.2. Augmented Jacobian Matrix Incorporating Line Temperature

With the augment of measurement and state variables, the Jacobian matrix $\boldsymbol{H}$ is also augmented. In order to determine the elements related to line temperatures, the augmented Jacobian matrix $\boldsymbol{H}_{aug}$ is partitioned, which can be represented as,

$$\boldsymbol{H}_{aug} = \frac{\partial \boldsymbol{h}(\boldsymbol{x})}{\partial \boldsymbol{x}} = \begin{bmatrix} \boldsymbol{H}_{11} & \boldsymbol{H}_{12} & \boldsymbol{H}_{13} \\ \boldsymbol{H}_{21} & \boldsymbol{H}_{22} & \boldsymbol{H}_{23} \end{bmatrix} = \begin{bmatrix} \partial \boldsymbol{h}_{RTU}/\partial \boldsymbol{U} & \partial \boldsymbol{h}_{RTU}/\partial \theta & \partial \boldsymbol{h}_{RTU}/\partial \boldsymbol{T} \\ \partial \boldsymbol{h}_{HBE}/\partial \boldsymbol{U} & \partial \boldsymbol{h}_{HBE}/\partial \theta & \partial \boldsymbol{h}_{HBE}/\partial \boldsymbol{T} \end{bmatrix} \tag{19}$$

Moreover, the submatrices $\boldsymbol{H}_{11}$ and $\boldsymbol{H}_{12}$ are identical to the Jacobian matrix of WLS-SE. Taking $\boldsymbol{H}_{23,i}$ as an example, the magnitude of a branch current flowing through the line l can be obtained directly via a current magnitude meter. Further, the partial differential coefficients corresponding to the line temperature T_l can be expressed as,

$$\boldsymbol{H}_{23,i} = \begin{bmatrix} & & & 0 & 0 & \\ \cdots & \vdots & \vdots & \vdots & \vdots & \cdots \\ & \frac{\partial U_i}{\partial T_l} & \frac{\partial \theta_i}{\partial T_l} & \frac{\partial I_{ij,real}}{\partial T_l} & \frac{\partial I_{ij,imag}}{\partial T_l} & \\ \cdots & \vdots & \vdots & \vdots & \vdots & \cdots \\ & & & 0 & 0 & \end{bmatrix}^T \tag{20}$$

with

$$\frac{\partial U_i}{\partial T_l} = 0 \tag{21}$$

$$\frac{\partial \theta_i}{\partial T_l} = 0 \tag{22}$$

$$\frac{\partial I_{ij,real}}{\partial T_l} = -(U_i \cos\theta_i - U_j \cos\theta_j)\frac{\partial G_{ij}(T_l)}{\partial T_l} + (U_i \sin\theta_i - U_j \sin\theta_j)\frac{\partial B_{ij}(T_l)}{\partial T_l} \tag{23}$$

$$\frac{\partial I_{ij,imag}}{\partial T_l} = -(U_i \cos\theta_i - U_j \cos\theta_j)\frac{\partial B_{ij}(T_l)}{\partial T_l} - (U_i \sin\theta_i - U_j \sin\theta_j)\frac{\partial G_{ij}(T_l)}{\partial T_l} \tag{24}$$

It should be noted that only when temperature T_l corresponds to transmission line l, is the partial differential coefficients not equal to 0, i.e., merely one element in each row of $\partial_{Iij,real}/\partial T$ and $\partial I_{ij,imag}/\partial T$ is not equal to 0.

Moreover, regarding the submatrix $\boldsymbol{H}_{31}$, at most two elements in each row are not equal to 0. Then, the submatrix $\boldsymbol{H}_{31}$ can be expressed as,

$$\boldsymbol{H}_{31,l} = \begin{bmatrix} 0 & \cdots & \frac{\partial h_{HBE,l}}{\partial U_i} & \cdots & 0 & \cdots & \frac{\partial h_{HBE,l}}{\partial U_j} & \cdots & 0 \end{bmatrix} \tag{25}$$

In addition, the corresponding partial differential coefficient is calculated as,

$$\frac{\partial h_{HBE,l}}{\partial U_i} = (G_{ij}^2 + B_{ij}^2)(2U_i - U_j \cos\theta_{ij})R \tag{26}$$

Similarly, in the submatrix $\boldsymbol{H}_{32}$, at most two elements in each row are not equal to 0, the submatrix $\boldsymbol{H}_{32}$ can be represented as,

$$\boldsymbol{H}_{32,l} = \begin{bmatrix} 0 & \cdots & \frac{\partial h_{HBE,l}}{\partial \theta_i} & \cdots & 0 & \cdots & \frac{\partial h_{HBE,l}}{\partial \theta_j} & \cdots & 0 \end{bmatrix} \tag{27}$$

Then, the corresponding partial differential coefficient is calculated as,

$$\frac{\partial h_{HBE,l}}{\partial \theta_i} = (G_{ij}^2 + B_{ij}^2)(2U_i U_j \sin\theta_{ij})R \tag{28}$$

Since the HBE of the transmission line l is merely relevant to the corresponding line temperature T_l, the submatrix $\boldsymbol{H}_{33}$ is a diagonal matrix and represented as,

$$\boldsymbol{H}_{33} = \begin{bmatrix} \ddots & & & 0 \\ 0 & \frac{\partial h_{HBE,l}}{\partial T_l} & \cdots & 0 \\ 0 & \cdots & \frac{\partial h_{HBE,m}}{\partial T_m} & 0 \\ 0 & & & \ddots \end{bmatrix} \tag{29}$$

with

$$\begin{aligned} \frac{\partial h_{HBE,l}}{\partial T_l} &= (2G_{ij}\frac{\partial G_{ij}}{\partial T_l} + 2B_{ij}\frac{\partial B_{ij}}{\partial T_l})(U_i^2 + U_j^2 - 2U_i U_j \cos\theta_{ij})R + \\ &(G_{ij}^2 + B_{ij}^2)\cdot(U_i^2 + U_j^2 - 2U_i U_j \cos\theta_{ij})\cdot\frac{\partial R}{\partial T_l} - A_c - 4A_r(T_l + 273)^3 \end{aligned} \tag{30}$$

$$\frac{\partial G_{ij}(T_l)}{\partial T_l} = \frac{\alpha_l R_{r,ij}^3[1 + \alpha_l(T_l - T_d)]^2 - \alpha_l R_{r,ij} X_{ij}^2}{\left\{R_{r,ij}^2[1 + \alpha_l(T_l - T_d)]^2 + X_{ij}^2\right\}^2} \tag{31}$$

$$\frac{\partial B_{ij}(T_l)}{\partial T_l} = \frac{-2\alpha_l X_{ij} R_{r,ij}^2[1 + \alpha_l(T_l - T_d)]}{\left\{R_{r,ij}^2[1 + \alpha_l(T_l - T_d)]^2 + X_{ij}^2\right\}^2} \tag{32}$$

3.3. Solving Approach for Augmented Jacobian ETC-SE

As aforementioned, the AJ-ETC-SE is an overdetermined equation set. With the augmented Jacobian matrix $\boldsymbol{H}$, the AJ-ETC-SE can be solved by the Newton method, as shown in Figure 2. Thus, the detailed solving procedures of the proposed AJ-ETC-SE approach can be listed as,

(1) Obtain system topology and network parameters.
(2) Input the measured electrical and meteorological data.
(3) Initialize the voltage phasors, line temperature, and corresponding parameters.
(4) Form the admittance matrix, and calculate the augmented Jacobian matrix $\boldsymbol{H}_{aug}$ according to (19)–(32).
(5) Calculate the correction vector $\Delta \boldsymbol{x}_{aug}$ by (36) and update the state vector $\boldsymbol{x}_{aug}$ by (18).
(6) If $\|\Delta \boldsymbol{x}_{aug}\|_{\infty} \leq \xi$, output the state vector $\boldsymbol{x}_{aug}$, otherwise, return to step (4).

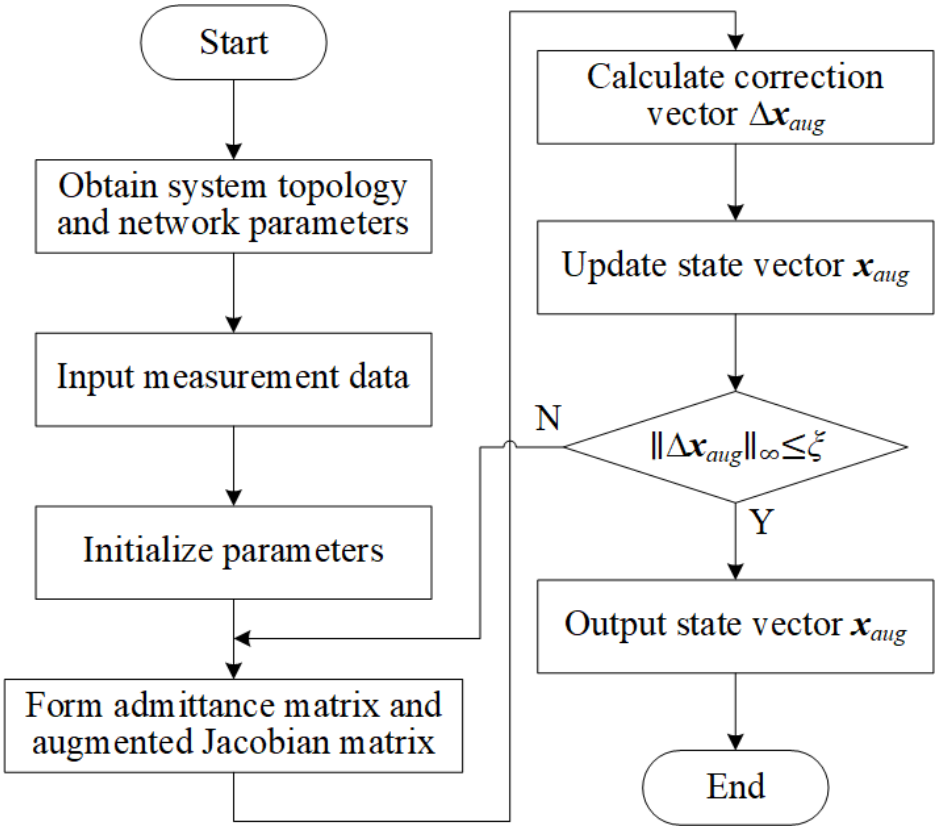

Figure 2. Flowchart of the proposed AJ-ETC-ES approach.

4. Improved Two-Step ETC-SE Approach

4.1. Framework of Improved Two-Step ETC-SE

The framework of the proposed ITS-ETC-SE approach can be illustrated in Figure 3. The SE and temperature estimation are decoupled and solved via alternate iteration. At each iteration, the SE is first conducted. The nodal voltage and line current are calculated, which serve as the input for calculating the HBE. Then, line temperature is calculated according to the outputs of SE and meteorological data, and utilized to modify line parameters and the admittance matrix for SE. The process is carried out repeatedly until both state variables and line temperatures converge.

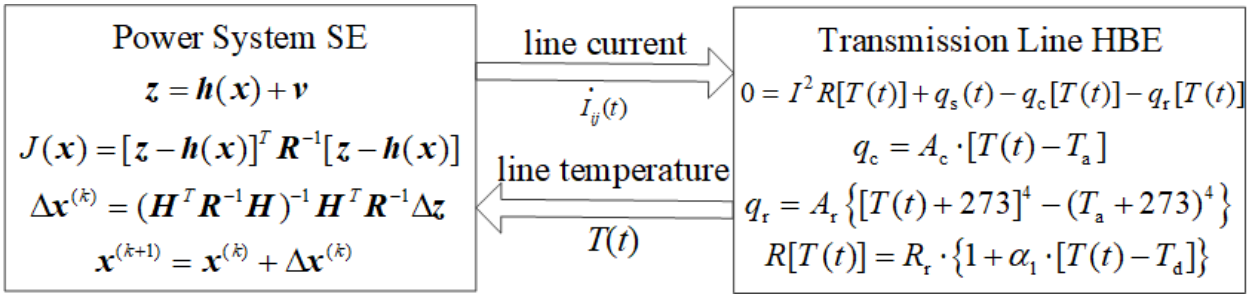

Figure 3. Framework of the proposed ITS-ETC-ES approach.

4.2. Procedure of Improved Two-Step ETC-SE

Similar to the proposed AJ-ETC-SE approach, the estimation of voltage phasors can be solved by the Newton method, and represented as,

$$\Delta \boldsymbol{x}_k = [\boldsymbol{H}^T(\boldsymbol{x}_k)\boldsymbol{R}^{-1}\boldsymbol{H}(\boldsymbol{x}_k)]^{-1}\boldsymbol{H}^T(\boldsymbol{x}_k)\boldsymbol{R}^{-1}\Delta \boldsymbol{z}_k \tag{33}$$

$$\boldsymbol{x}_{k+1} = \boldsymbol{x}_k + \Delta \boldsymbol{x}_k \tag{34}$$

Furthermore, according to (9)–12), the HBE can be rearranged as,

$$\begin{aligned} &f(T) = I^2 R(T) + q_s - q_r(T) - q_c(T) = \\ &I^2 R_r[1 + \alpha_l(T - T_d)] + q_s - A_r[(T + 273)^4 - (T_a + 273)^4] - A_c(T - T_a) = 0 \end{aligned} \tag{35}$$

where A_r and A_c are coefficients of radiated heat loss and convective heat loss, respectively.

In the (k+1)th iteration, the estimation of line temperature can be calculated by the Newton method. According to (35), the calculation process can be represented as,

$$T_{k+1} = T_k + \Delta T_k = T_k - \frac{f(T_k)}{f'(T_k)} \tag{36}$$

$$f'(T_k) = \alpha_l I_{k+1}^2 R_r - 4A_r(273 + T_k)^3 - A_c \tag{37}$$

$$I_{ij,k+1}^2 = [G_{ij,k}^2(T_k) + B_{ij,k}^2(T_k)](U_{i,k+1}^2 + U_{j,k+1}^2 - 2U_{i,k+1}U_{j,k+1}\cos\theta_{ij,k+1}) \tag{38}$$

With the combination of the (17), (18), and (36)–(38), the procedures of the proposed ITS-ETC-SE approach can be demonstrated in Figure 4, and listed as,

(1) Obtain system topology and network parameters.
(2) Input the measured electrical and meteorological data.
(3) Initialize the voltage phasors, line temperature, and corresponding parameters.
(4) Form the admittance matrix and Jacobian matrix, calculate the correction vector $\Delta \boldsymbol{x}$ by (33), and update the state vector $\boldsymbol{x}$ by (34).
(5) Calculate the current of transmission lines by (38), and the correction vector of temperature $\Delta \boldsymbol{T}$ by (36) and (37).
(6) If $\|\Delta \boldsymbol{x}\|_\infty \leq \xi$ and $\|\Delta T\|_\infty \leq \xi$, output the state vector $\boldsymbol{x}$, otherwise, update the line parameters according to (31) and (32), and return to step (4).

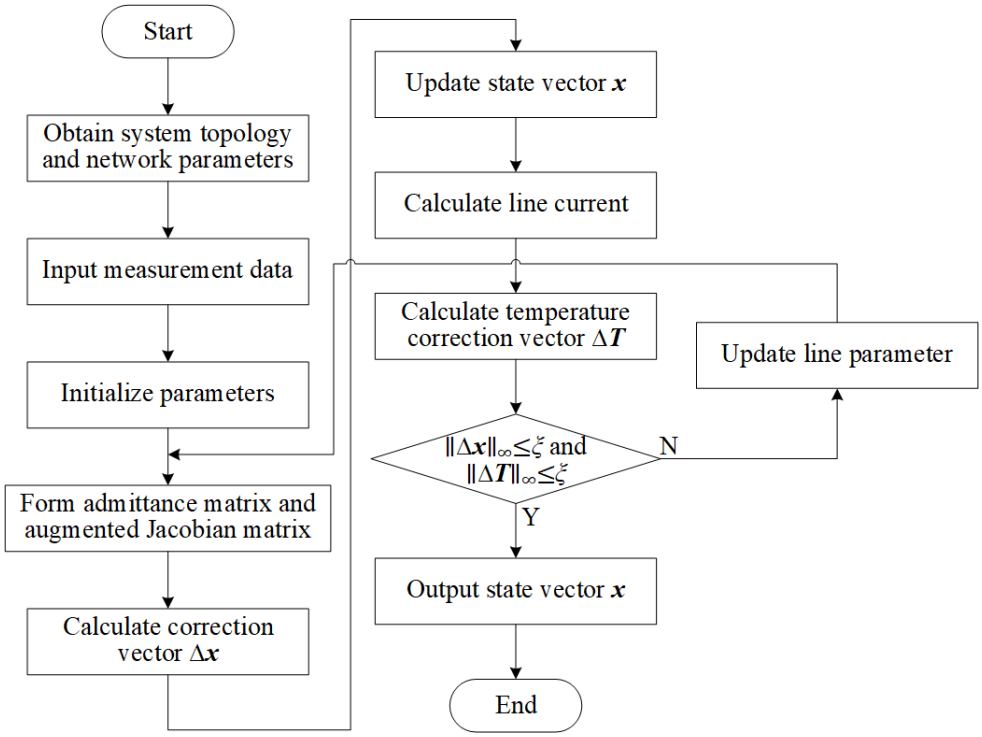

Figure 4. Flowchart of the proposed ITS-ETC-ES approach.

5. Case Studies

The IEEE 14-, 39-, and 118-bus systems are utilized to verify the effectiveness of the proposed AJ-ETC-SE and ITS-ETC-SE approaches. The WLS-SM method in [19] is used for comparison. Moreover, the algorithms are developed on the MATLAB R2019b. Further, the calculation is conducted on a 2.33 GHz Intel (R) Core (TM) 2 Quad CPU Q8200 processor with 16 GB of RAM. Additionally, the convergence threshold ξ, for the Newton method is set as 0.0001.

Voltage amplitude, power injection, branch power flow, and currents are incorporated in the measurement vector. Then, 2% and 4% Gaussian-distributed white noise are added to the voltage and power measurements, respectively. Meteorological parameters remain constant, which is reasonable for the short simulation time.

Furthermore, the root mean square (RMS) error of estimation results e_{RMS} is calculated, and can be expressed as,

$$e_{RMS} = \sqrt{\frac{1}{NM}\sum_{i=1}^{N}\sum_{j=1}^{M}\left(\frac{x_j - x_{ij,r}}{x_j}\right)^2} \tag{39}$$

where N is the group of measurement data, M is the number of buses, $\boldsymbol{x}_j$ is the value of the jth state variable, and $\boldsymbol{x}_{i,j,r}$ is the estimated value of the jth state variable with the ith group of measurement data.

5.1. Estimation Results of Proposed ETC-SE Approach

The simulation and estimation of the three systems are conducted 10,000 times. The probability density functions (PDFs) of the estimated voltage U_1 with the proposed AJ- and ITS-ETC-SE approaches are depicted in Figure 5. For comparison, the PDF of the WLS-SE method is also depicted.

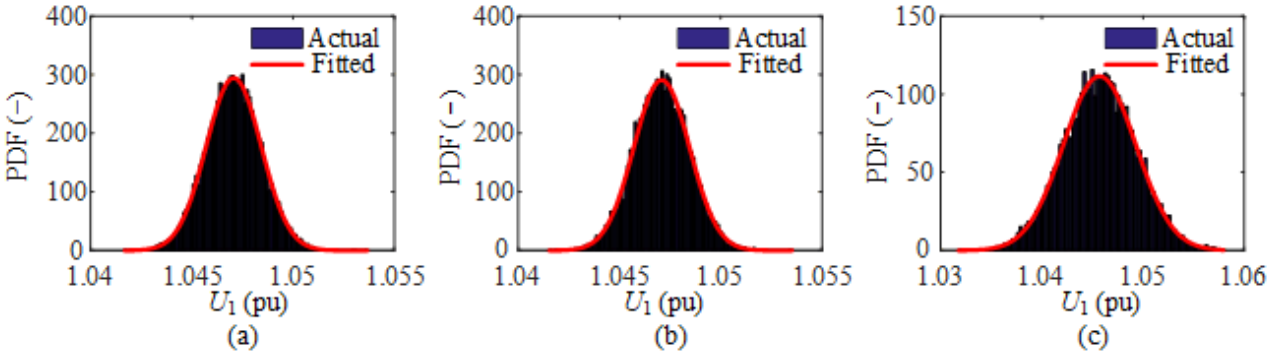

Figure 5. PDF of estimated voltage U_1 with different methods. (**a**) ITS-ETC-SE approach, (**b**) AJ-ETC-SE approach, (**c**) WLS-SE method.

Table 2 shows the RMS and maximum estimated errors of the 10,000 samples with different methods. The errors of the proposed ETC-SE approaches are almost the same and smaller than the errors of the WLS-SE method, whose voltage amplitude and phase angle errors are merely 0.13% and 6.18%, respectively. In addition, the averaged voltage errors of the IEEE 39-bus system with the proposed ITS-ETC-SE approach and WLS-SE method can be depicted in Figure 6. The temperatures are considered in the ITS-ETC-SE method but not in the WLS-SE method. Due to the influence of variable temperatures, the fluctuations of the WLS-SE method are more serious than the ITS-ETC-SE method.

Table 2. Estimated errors with different methods.

Method		ITS-ETC-SE	AJ-ETC-SE	WLS-SE
Voltage amplitude	$e_{U,\mathrm{RMS}}$ (%)	0.13	0.13	0.41
	$e_{U\max}$ (%)	0.63	0.58	1.54
Phase angle	$e_{\theta,\mathrm{RMS}}$ (%)	6.18	6.23	6.48
	$e_{\theta\max}$ (%)	27.66	28.03	44.20
Line temperature	$e_{T,\mathrm{RMS}}$ (%)	0.86	0.85	\
	$e_{T\max}$ (%)	2.26	2.23	\
Active power	$e_{P,\mathrm{RMS}}$ (%)	4.99	4.98	5.32
	$e_{P\max}$ (%)	39.70	32.88	42.02
Reactive power	$e_{Q,\mathrm{RMS}}$ (%)	5.43	5.40	6.51
	$e_{Q\max}$ (%)	31.36	37.73	36.57

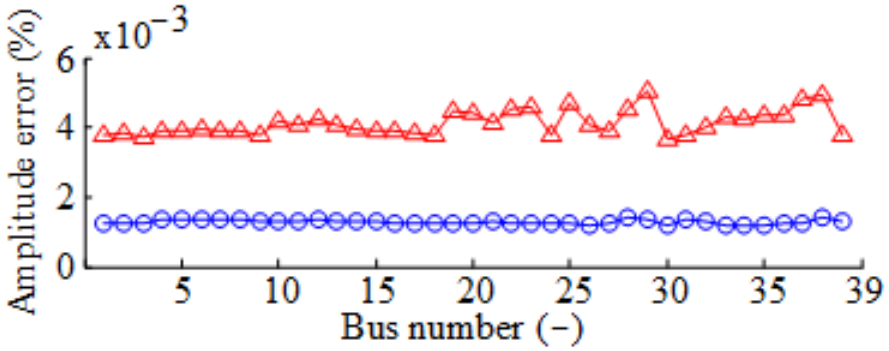

Figure 6. Averaged voltage errors of the IEEE 39-bus system.

Furthermore, the estimated temperature and power loss of transmission lines in the IEEE 39-bus system are demonstrated in Table 3. It is obvious that the temperature varies greatly on different lines, ranging from 34 °C to 68 °C, which is affected by branch power

flow. Similar results have been obtained in power loss, with an increase over 10% in the proposed ITS-ETC-SE approach compared with the WLS-SE method.

Table 3. Estimated results of the IEEE 39-bus system.

Branch	Power Loss of WLS-SE (pu)	Power Loss of ITS-ETC-SE (pu)	Power Loss Change (%)	T (°C)
1–2	4.742×10^{-3}	4.994×10^{-3}	5.32	38.08
1–39	1.355×10^{-3}	1.433×10^{-3}	5.751	39.2
2–3	1.669×10^{-2}	1.879×10^{-2}	12.61	54.55
2–25	3.925×10^{-2}	4.397×10^{-2}	12.02	50.8
3–4	2.228×10^{-3}	2.348×10^{-3}	5.372	39.89
3–18	1.475×10^{-4}	1.561×10^{-4}	5.825	34.89
4–5	2.112×10^{-3}	2.351×10^{-3}	11.27	42.03
4–14	5.646×10^{-3}	6.409×10^{-3}	13.51	54.53
5–6	4.638×10^{-3}	5.355×10^{-3}	15.45	56.55
5–8	8.27×10^{-3}	9.746×10^{-3}	17.84	65.14
6–7	1.122×10^{-2}	1.264×10^{-2}	12.65	51.22
6–11	8.241×10^{-3}	9.753×10^{-3}	18.35	68.97
7–8	1.47×10^{-3}	1.624×10^{-3}	10.49	44.89
8–9	2.702×10^{-3}	2.957×10^{-3}	9.448	36.84
9–39	4.956×10^{-4}	5.452×10^{-4}	10.01	34.65
10–11	4.867×10^{-3}	5.282×10^{-3}	8.539	43.5
10–13	3.601×10^{-3}	4.205×10^{-3}	16.77	60.95
13–14	7.677×10^{-3}	8.917×10^{-3}	16.15	59.35
14–15	4.692×10^{-4}	4.829×10^{-4}	2.917	34.98
15–16	9.33×10^{-3}	1.085×10^{-2}	16.3	63.86
16–17	2.903×10^{-3}	3.179×10^{-3}	9.518	45.93
16–19	3.107×10^{-2}	3.64×10^{-2}	17.14	64.25
16–21	8.176×10^{-3}	9.587×10^{-3}	17.25	64.56
16–24	3.177×10^{-4}	3.332×10^{-4}	4.871	37.24
17–18	2.438×10^{-3}	2.677×10^{-3}	9.8	44.33
17–27	2.365×10^{-4}	2.525×10^{-4}	6.772	34.79
21–22	2.803×10^{-2}	3.253×10^{-2}	16.08	61.32
22–23	1.969×10^{-4}	2.068×10^{-4}	5.003	35.7
23–24	2.524×10^{-2}	2.999×10^{-2}	18.81	68.48
25–26	1.8×10^{-3}	1.963×10^{-3}	9.05	36.11
26–27	9.707×10^{-3}	1.115×10^{-2}	14.83	55.09
26–28	7.906×10^{-3}	8.453×10^{-3}	6.92	39.59
26–29	1.899×10^{-2}	2.071×10^{-2}	9.078	43.88
28–29	1.543×10^{-2}	1.827×10^{-2}	18.39	67.25

Estimated errors of line resistance and temperature in the IEEE 39-bus system are demonstrated in Figure 7. Line resistance errors refer to the deviation between the actual resistance and its rated value. Compared with its rated values, the actual values of most line resistance increase over 10% when taking ETC into account. The resistance errors of the WLS-SE method are over 10% and the maximum error even reaches 19.1%. Estimated temperature error of most lines with the proposed ETC-SE approaches are less than 1%. Furthermore, the voltage and temperature errors of the IEEE 118-bus system are depicted in Figure 8.

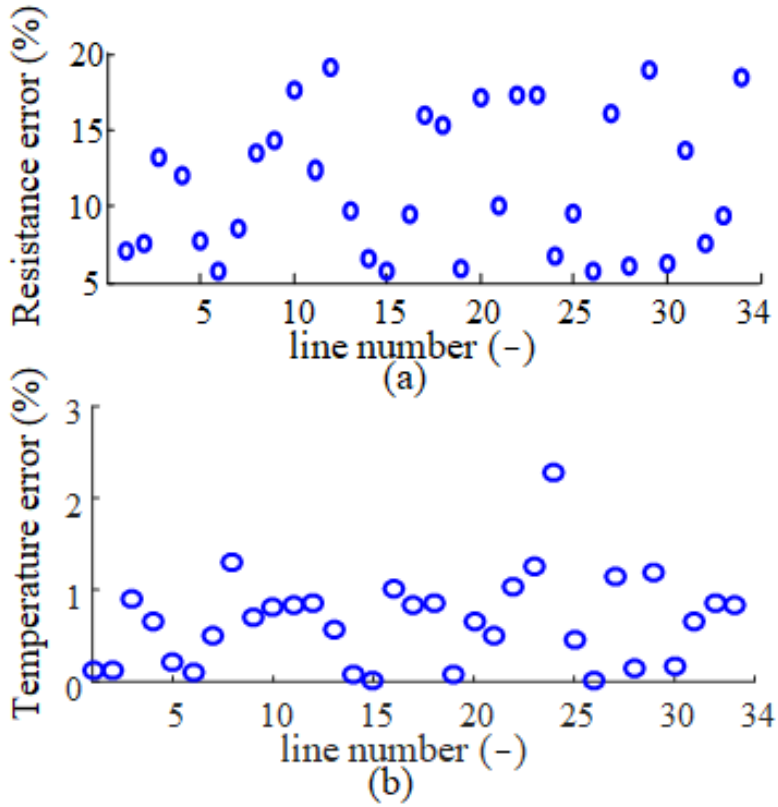

Figure 7. Resistance and line temperature error of the IEEE 39-bus system. (**a**) Resistance error, (**b**) temperature error.

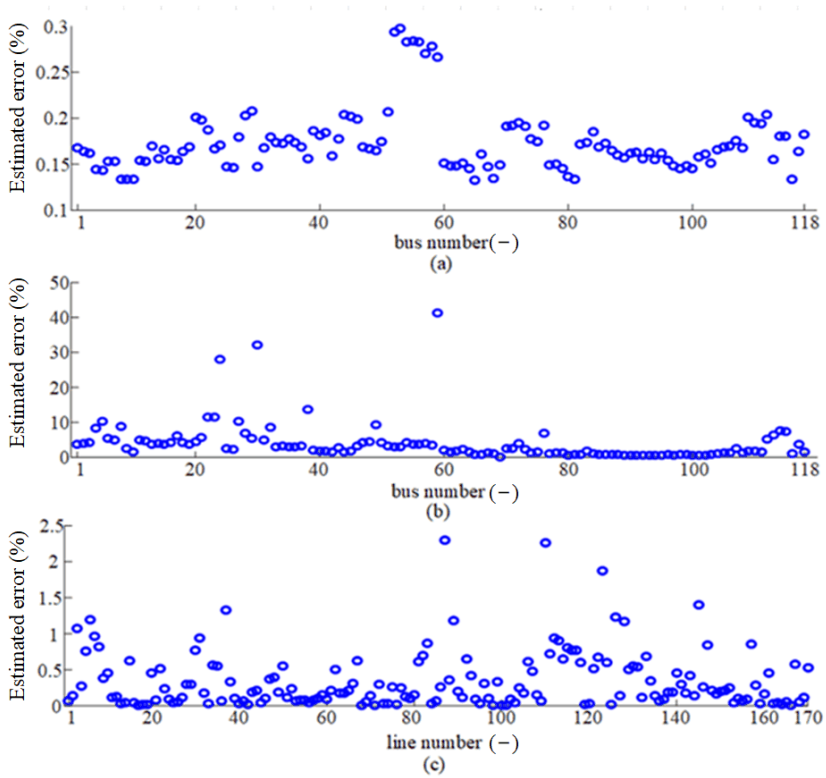

Figure 8. Resistance and line temperature error of the IEEE 118-bus system. (**a**) Voltage amplitude error, (**b**) phase angle error, (**c**) line temperature error.

5.2. Performance Analysis

A comparison of the computation time and iteration numbers on the proposed ETC-SE approaches and WLS-SE method was performed, as shown in Table 4. The ETC-SE approaches need more iteration numbers than the WLS-SE method. Line temperature converges more slowly than state variables. As for the computation time, the proposed ITS-ETC-SE approach is shorter than the AJ-ETC-SE approach.

Table 4. Comparison of iteration numbers and computation time.

Method		ITS-ETC-SE	AJ-ETC-SE	WLS-SE
Iteration numbers	14-bus	6	6	4
	39-bus	6	6	4
	118-bus	7	8	4
Computation time (s)	14-bus	0.057	0.141	0.018
	39-bus	0.089	0.264	0.037
	118-bus	0.966	3.432	0.316

Table 5 shows the computational complexity of the AJ-ETC-SE approach and WLS-SE method. With the consideration of line temperature, the number of measurements and state variables, and the dimension of the Jacobian matrix increase sharply and even over 100% compared with the WLS-SE method.

Table 5. Comparison of computational complexity of the AJ-ETC-SE approach and WLS-SE method.

Index		14-Bus	39-Bus	118-Bus
Number of ETC lines		15	34	170
Number of States	WLS-SE	27	77	235
	AJ-ETC-SE	42	111	405
	Change (%)	55.6	44.2	72.3
Number of measurements	WLS-SE	42	165	403
	AJ-ETC-SE	57	199	573
	Change (%)	35.7	20.6	42.2
Dimension of Jacobian matrix	WLS-SE	42 × 27	165 × 77	403 × 235
	AJ-ETC-SE	57 × 42	199 × 111	573 × 405
	Change (%)	111.1	73.9	145.0

Figure 9 shows the maximum unbalance of state variables $\|\Delta x\|_\infty$ during each iteration. It can be seen that the index $\|\Delta x\|_\infty$ first declines linearly, and then nearly remains constant.

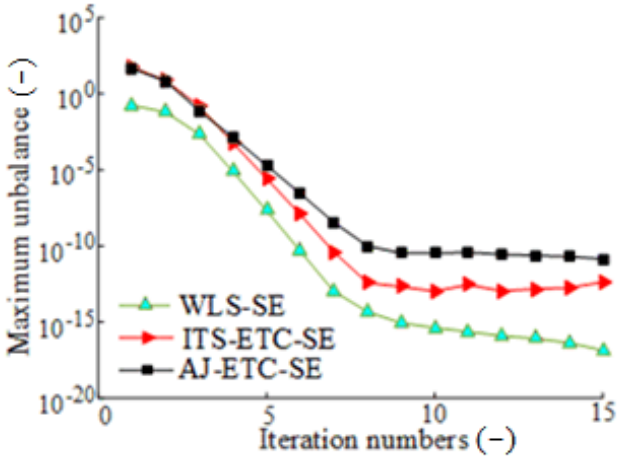

Figure 9. Maximum unbalance of state variables.

Furthermore, different scenarios are conducted in order to explore the convergence performance of the proposed ETC-SE approaches, including varying environmental conditions and the existence of ill-conditioned branches. For each scenario, 1000 simulations are performed in the IEEE 118-bus system.

The environmental conditions vary with the ambient temperature T_a and wind velocity V_w. More specially, the ambient temperature T_a increases from 25 °C to 50 °C and the wind velocity V_w increases from 1 m/s to 20 m/s, which will lead to changes in convective heat loss q_c. The iteration numbers of the proposed ETC-SE approaches can be summarized in Tables 6 and 7, respectively.

Table 6. Iteration numbers of different algorithms under different ambient temperatures.

T_a (°C)	ITS-ETC-SE	AJ-ETC-SE
25	7	8
35	7	8.04
40	7.01	8.21
45	7.02	8.43
50	7.02	8.69

Table 7. Iteration numbers of different algorithms under different wind velocities.

V_w (m/s)	ITS-ETC-SE	AJ-ETC-SE
1	7	8
2	6.98	7.38
5	6	6.47
10	6	5.59
20	5.2	5.01

Furthermore, the ill-conditioned branches are added to the IEEE 118-bus system. Moreover, the ill-conditioned branches refer to the high-resistance branches whose $R = 0.5X$. The iteration numbers of the proposed ETC-SE approaches are shown in Table 8.

Table 8. Iteration numbers with ill-conditioned branches.

Number of Ill-Conditioned Lines	ITS-ETC-SE	AJ-ETC-SE
1	7	8
3	7	8.53
5	7	8.60
8	7.03	8.61
10	7.05	8.63

6. Discussion

The proposed approach is to estimate the power system states considering electro-thermal coordination, and the calculation results include the power system states and transmission line temperature. The performance of the proposed approach in terms of efficiency, effectiveness, and accuracy can be verified by the comparison analysis in the above case study.

From Figure 5, it is clear that the PDFs with the proposed ETC-SE approaches are nearly identical and more concentrated compared with the WLS-SE method. Additionally, compared to the WLS-SE method, the results in Table 2 and Figure 6 show that the proposed AJ- and ITS-ETC-SE approach is effective to decrease the errors. Moreover, the iteration numbers and computation time are compared in Table 4. The results show that the proposed ITS-ETC-SE approach is effective in accelerating the solving process. Since the dimension of the measurement vector, state vector, and Jacobian matrix increases to a larger extent after integrating line temperature into the SE model, the computation time of the AJ-ETC-SE approach is much longer than the ITS-ETC-SE approach and WLS-SE method.

Figure 9 verifies the superior computational performance of the ITS-ETC-SE approach when compared to the AJ-ETC-SE approach. Furthermore, the sensitivity analysis is conducted by considering different scenarios in terms of ambient temperature, wind velocity, and ill-conditioned branches. The iteration numbers of different methods are summarized in Tables 6–8, and the results show that the proposed ETC-SE approaches show good convergence performance with environmental condition variation and ill-conditioned branches. The iteration numbers increase as the ambient temperature increases and wind velocity declines. Moreover, reliable convergence can also be achieved when ill-conditioned branches exist, and there are merely tiny increases in iteration numbers, which will facilitate the utilization of the proposed ETC-SE approaches in practical application.

7. Conclusions

The SE considering the influence of line temperature is studied, and the ETC-SE approaches are proposed to reduce the temperature-dependent errors. An ETC-SE model integrating the HBE and WLS-SE is established. In addition, the AJ-ETC-SE approach is presented to simultaneously solve the problems of SE and temperature estimation through an augmented Jacobian matrix. For the sake of accelerating the solving process, the ITS-ETC-SE approach is proposed, in which the SE and temperature estimation are decoupled and solved via alternate iteration.

The effectiveness, efficiency, and convergence performance of the proposed ETC-SE approaches are verified through the IEEE 14-, 39-, and 118-bus systems. Results show that the proposed ETC-SE approaches can reduce estimated errors evidently and estimate line temperature precisely. The accuracy of the AJ-ETC-SE approach is slightly higher than the ITS-ETC-SE approach. Further, the ITS-ETC-SE approach is able to accelerate the calculation process. Furthermore, the ETC-SE approaches possess good convergence performance with varying environmental circumstances and ill-conditioned branches.

In future studies, the influence of the measurements of PMUs on the SE will be considered, and an ETC-SE approach will be provided based on hybrid measurement data.

Author Contributions: Conceptualization, Y.C. and H.Z.; methodology, Y.C.; software, Q.X.; writing—original draft preparation, Q.X. and Z.G.; writing—review and editing, H.Q. and Q.X.; supervision, Y.C. and H.Z. All authors have read and agreed to the published version of the manuscript.

Funding: This paper is funded by Shandong Provincial Natural Science Foundation (No. ZR2021QE133).

Conflicts of Interest: The authors declare no conflict of interest.

Nomenclature

PMU	phasor measurement unit
ETC	electro-thermal coordination
HBE	heat balance equation
RTU	remote terminal unit
SE	state estimation
PMSM	permanent magnet synchronous motor
EVB	electric vehicle battery
AJ-ETC-SE	augmented Jacobian ETC-SE
WLS-SE	weighted least square SE
ITS-ETC-SE	improved two-step ETC-SE
PDF	probability density function
P_i and Q_i	the active and reactive power injection of bus i, respectively
P_j and Q_j	the active and reactive power injection of bus j, respectively
P_{ij} and Q_{ij}	the active and reactive power flow of the line l, respectively
U_i and U_j	the voltage amplitudes of bus i and j, respectively
$I_{ij,real}$ and $I_{ij,imag}$	the real and image parts of the current from bus i to bus j, respectively
$I_{ji,real}$ and $I_{ji,imag}$	the real and image parts of the current from bus j to bus i, respectively

g_{ij} and b_{ij}	the mutual conductance and susceptance of the line l, respectively
$g_{ij,c}$ and $b_{ij,c}$	the self-conductance and susceptance of the line l, respectively
z_{elec} and z_{meteo}	the measurement vectors of electrical and meteorological quantities, respectively
Q_{solar}, ϑ, V_w, T_a and ϕ	the solar irradiation intensity, solar incidence angle, wind speed, ambient temperature, and wind directions, respectively
h_{aug}	the augmented measurement function vector
h_{elec} and h_{HBE}	the measurement function vectors of electrical and HBE, respectively
U, θ and T	the voltage magnitude, voltage angle, and line temperature vectors, respectively
R	the unit resistance of transmission line
q_s, q_c and q_r	the solar heat gain, convective heat loss and radiated heat loss, respectively
A_c and A_r	the coefficients for convective heat loss and radiated heat loss, respectively
α	the temperature coefficient of resistance
T_d	the reference temperature
R_r	the rated resistance
Δx_{aug} and $H(x_{aug,0})$	the correction vector and Jacobian matrix, respectively
R	the weighting matrix
A_r and A_c	the coefficients of radiated heat loss and convective heat loss, respectively

References

1. Xu, Q.; Cao, Y.; Zhang, H.; Zhang, W.; Terzija, V. Bi-level dispatch and control architecture for power system in China based on grid-friendly virtual power plant. *Appl. Sci.* **2021**, *11*, 1282. [CrossRef]
2. Abdelsalam, M.; Diab, H.Y.; El-Bary, A.A. A metaheuristic harris hawk optimization approach for coordinated control of energy management in distributed generation based Microgrids. *Appl. Sci.* **2021**, *11*, 4085. [CrossRef]
3. Cao, Y.; Zhang, Y.; Zhang, H.; Shi, X.; Terzija, V. Probabilistic optimal PV capacity planning for wind farm expansion based on NASA data. *IEEE Trans. Sustain. Energy* **2017**, *8*, 1291–1300. [CrossRef]
4. Cao, Y.; Wu, Q.; Zhang, H.; Li, C.; Zhang, X. Chance-constrained optimal configuration of BESS considering uncertain power fluctuation and frequency deviation under contingency. *IEEE Trans. Sustain. Energy* **2022**, *13*, 2291–2303. [CrossRef]
5. Elyasichamazkoti, F.; Teimourzadeh, S.; Aminifar, F. Optimal distribution of power grid under-frequency load shedding with security considerations. *IEEE Trans. Power Syst.* **2022**, *37*, 4110–4112. [CrossRef]
6. Xu, X.; Cao, Y.; Zhang, H.; Ma, S.; Song, Y.; Chen, D. A multi-objective optimization approach for corrective switching of transmission systems in emergency scenarios. *Energies* **2017**, *10*, 1204. [CrossRef]
7. Yang, H.; Qiu, R.C.; Chu, L.; Mi, T.; Shi, X.; Liu, C.M. Improving power system state estimation based on matrix-level cleaning. *IEEE Trans. Power Syst.* **2020**, *35*, 3529–3540. [CrossRef]
8. Ban, J.; Im, J.; Kim, Y.; Zhao, J. Decentralization of phasor-aided state estimation using local state vector extension. *IEEE Trans. Power Syst.* **2021**, *36*, 4645–4659. [CrossRef]
9. Asprou, M.; Kyriakides, E.; Albu, M. The effect of parameter and measurement uncertainties on hybrid state estimation. In Proceedings of the IEEE Power and Energy Society General Meeting, San Diego, CA, USA, 22–26 July 2012; pp. 1–7.
10. Zhao, J.; Gómez-Expósito, A.; Netto, M.; Mili, L.; Abur, A.; Terzija, V.; Kamwa, I.; Pal, B.; Singh, A.K.; Qi, J.; et al. Power system dynamic state estimation: Motivations, definitions, methodologies, and future work. *IEEE Trans. Power Syst.* **2019**, *34*, 3188–3198. [CrossRef]
11. Santos, J.R.; Expósito, A.G.; Sánchez, F.P. Assessment of conductor thermal models for grid studies. *IET Gener. Transm. Distrib.* **2007**, *1*, 155–161. [CrossRef]
12. Asprou, M.; Kyriakides, E. Identification and estimation of erroneous transmission line parameters using PMU measurements. *IEEE Trans. Power Deliv.* **2017**, *32*, 2510–2519.
13. Banakar, H.; Alguacil, N.; Galiana, F.D. Electrothermal coordination part I: Theory and implementation schemes. *IEEE Trans. Power Syst.* **2005**, *20*, 798–805. [CrossRef]
14. *IEEE Std 738-2006*; IEEE Standard for Calculating the Current-Temperature of Bare Overhead Conductors. IEEE: New York, NY, USA, 2007.
15. Ali, M.; Degefa, M.Z.; Humayun, M.; Safdarian, A.; Lehtonen, M. Increased utilization of wind generation by coordinating the demand response and real-time thermal rating. *IEEE Trans. Power Syst.* **2016**, *31*, 3737–3746. [CrossRef]
16. Douglass, D.; Chisholm, W.; Davidson, G.; Grant, I.; Lindsey, K.; Lancaster, M.; Lawry, D.; McCarthy, T.; Nascimento, C.; Pasha, M.; et al. Real-time overhead transmission-line monitoring for dynamic rating. *IEEE Trans. Power Deliv.* **2016**, *31*, 921–927. [CrossRef]
17. Cong, Y.; Regulski, P.; Wall, P.; Osborne, M.; Terzija, V. On the use of dynamic thermal-line ratings for improving operational tripping schemes. *IEEE Trans. Power Deliv.* **2016**, *31*, 1891–1900. [CrossRef]
18. Frank, S.; Sexauer, J.; Mohagheghi, S. Temperature-dependent power flow. *IEEE Trans. Power Syst.* **2013**, *28*, 4007–4018. [CrossRef]

19. Alguacil, N.; Banakar, H.; Galiana, F.D. Electrothermal coordination part II: Case studies. *IEEE Trans. Power Syst.* **2005**, *20*, 1738–1745. [CrossRef]
20. Cao, J.; Du, W.; Wang, H.F. Weather-based optimal power flow with wind farms integration. *IEEE Trans. Power Syst.* **2016**, *31*, 3073–3081. [CrossRef]
21. Bockarjova, M.; Andersson, G. Transmission line conductor temperature impact on state estimation accuracy. In Proceedings of the 2007 IEEE Lausanne Power Tech, Lausanne, Switzerland, 1–5 July 2007; pp. 701–706.
22. Yao, R.; Sun, K.; Liu, F.; Mei, S. Efficient simulation of temperature evolution of overhead transmission lines based on analytical solution and NWP. *IEEE Trans. Power Deliv.* **2017**, *33*, 1576–1588. [CrossRef]
23. Schlapfer, M.; Mancarella, P. Probabilistic modeling and simulation of transmission line temperatures under fluctuating power flows. *IEEE Trans. Power Deliv.* **2016**, *26*, 2235–2243. [CrossRef]
24. Rakpenthai, C.; Uatrongjit, S. Power system state and transmission line conductor temperature estimation. *IEEE Trans. Power Syst.* **2017**, *32*, 1818–1827. [CrossRef]
25. Jovicic, A.; Hug, G. Linear state estimation and bad data detection for power systems with RTU and PMU measurements. *IET Gener. Transm. Distrib.* **2020**, *14*, 5675–5684. [CrossRef]
26. Kabiri, M.; Amjady, N. Robust optimisation-based state estimation considering parameter errors for systems observed by phasor measurement units. *IET Gener. Transm. Distrib.* **2018**, *12*, 1915–1921. [CrossRef]
27. Zheng, W.; Wu, W.; Gomez-Exposito, A.; Zhang, B.; Guo, Y. Distributed robust bilinear state estimation for power systems with nonlinear measurements. *IEEE Trans. Power Syst.* **2016**, *32*, 499–509. [CrossRef]
28. Ho, C.H.; Wu, H.C.; Chan, S.C.; Hou, Y. A robust statistical approach to distributed power system state estimation with bad data. *IEEE Trans. Smart Grid* **2019**, *11*, 517–527. [CrossRef]
29. Gholami, M.; Abbaspour, A.; Fattaheian-Dehkordi, S.; Lehtonen, M.; Moeini-Aghtaie, M.; Fotuhi, M. Optimal allocation of PMUs in active distribution network considering reliability of state estimation results. *IET Gener. Transm. Distrib.* **2020**, *14*, 3641–3651. [CrossRef]
30. Zargar, S.F.; Farsangi, M.M.; Zare, M. Probabilistic multi-objective state estimation-based PMU placement in the presence of bad data and missing measurements. *IET Gener. Transm. Distrib.* **2020**, *14*, 3042–3051. [CrossRef]
31. Shahzad, K.; Jawad, M.; Ali, K.; Akhtar, J.; Khosa, I.; Bajaj, M.; Elattar, E.E.; Kamel, S. A hybrid approach for an efficient estimation and control of permanent magnet synchronous motor with fast dynamics and practically unavailable measurements. *Appl. Sci.* **2022**, *12*, 4958. [CrossRef]
32. Hossain, M.J.; Naeini, M. Multi-area distributed state estimation in smart grids using data-driven Kalman filters. *Energies* **2022**, *15*, 7105. [CrossRef]
33. Rahimifard, S.; Habibi, S.; Goward, G.; Tjong, J. Adaptive smooth variable structure filter strategy for state estimation of electric vehicle batteries. *Energies* **2021**, *14*, 8560. [CrossRef]